Phosphine-Stabilized Nickel–Sulfide Clusters as Electrocatalysts for Selective Aqueous Nitrate-to-Ammonium Conversion

Assistant Lecturer Maad Nafea Shakir Mahmoud
Open Educational College / Al-Dujail Branch
maad.nafea.alahbaby@ec.edu.iq

الملخص

يُعد الاختزال الكهربائي الانتقائي للنترات المائية إلى أمونيوم مسارًا جذابًا لمعالجة النيتروجين وتثمينه (الاستفادة منه) ومع ذلك، غالبًا ما تُظهر محفزات كبريتيد النيكل التقليدية (NiS_x) انتقالًا بطيئًا للشحنة البينية وقدرة غير مكتملة على الاحتفاظ بالانتقائية تحت الاستقطاب المستمر. في هذه الدراسة، تم تصنيع عناقيد النيكل–كبريت المثبتة بالفوسفين، [Ni_٤S_٤(PR_٣)_٤] ، تحت ظروف اختزالية، وتم تثبيتها على أقطاب عمل خاملة باستخدام استراتيجيات الإرساء السطحي (Surface–anchoring) التي تهدف إلى الحفاظ على سلامة العناقيد. كما تم تحضير راسب NiS_x تقليدي وترسيبه كغشاء رقيق ليكون بمثابة عينة ضابطة للمقارنة.

أكدت عملية التحقق قبل التحليل الكهربائي ـ والتي تجمع بين مقاييس التركيب العنصري (Ni, S, P) واكتشاف واسمات الرُبيطة(Ligand) ، وتحديد الطور — أن أقطاب العناقيد احتفظت بالبصمات التشخيصية للفوسفين وكانت متميزة كيميائيًا عن أغشية NiS_x. أتاح التخصيص على مستوى القطب (n=٢٥ لكل مجموعة) إجراء مقارنة مباشرة للتباين. وعلى الرغم من تقارب المساحة الهندسية، أظهرت أقطاب العناقيد مقاييس مرتفعة مرتبطة بالفوسفور تتوافق مع تثبيت العناقيد الحاملة للرُبيطات، في حين كانت العينات الضابطة خالية فعليًا من الفوسفور.

أظهرت الواسمات الثنائية فصلاً كاملاً: حيث ظهرت إشارات نطاق الفوسفين في مطيافية الأشعة تحت الحمراء (FTIR) وإشارات الرنين المغناطيسي النووي للفوسفور القابلة للكشف (P NMR{٣١}^) في جميع أقطاب العناقيد، بينما لم تظهر في أي من العينات الضابطة.

في إلكتروليت النترات، أظهرت أقطاب العناقيد بداية مبكرة لاختزال النترات (جهد بدء أقل سلبية) ومقاومة أقل لانتقال الشحنة، مما يشير إلى تحسن في الحركية البينية

(Interfacial kinetics)عند مقاومة محلول مماثلة. لم تختلف كثافة التيار عند جهد التقييم الثابت بشكل موثوق بين المجموعتين، مما يؤكد أن التحسن لم يكن ناتجًا عن زيادة في إجمالي التيار الكاثودي. بشكل عام، تدعم هذه الأدلة علاقة البنية بالنشاط (Structure–activity relationship)؛ حيث تُعزز التراكيب العنقودية السليمة للنيكل–كبريت المثبتة بالرُبيطات، وبيئتها السطحية الحاوية للفوسفور، انتقالًا أكثر ملاءمة للشحنة وتنشيطًا مبكرًا لتحويل النترات إلى أمونيوم بشكل يفوق أغشية NiS_x التقليدية.

الكلمات المفتاحية:

عناقيد كبريتيد النيكل، التثبيت بالفوسفين (أو الاستقرار بواسطة الفوسفين) ، التحفيز الكهربائي ،اختزال النترات (اختزال –NO_٣^٨)

Abstract

Selective aqueous nitrate electroreduction to ammonium is an attractive route for nitrogen remediation and valorization, yet conventional nickel sulfide (NiS(_x)) catalysts often exhibit sluggish interfacial charge transfer and imperfect selectivity retention under sustained polarization. Here, phosphine-stabilized nickel–sulfur clusters, [Ni(_٤)S(_٤)(PR(_٣))(_٤)], were synthesized under reducing conditions and immobilized on inert working electrodes using surface-anchoring strategies intended to preserve cluster integrity. A conventional NiS(_x) precipitate was prepared and deposited as a thin-film control. Pre-electrolysis verification—combining elemental composition metrics (Ni, S, P), ligand-marker detection, and phase identification—confirmed that cluster electrodes retained diagnostic phosphine signatures and were chemically distinct from NiS(_x) films. Electrode-level allocation (n=٢٥ per group) enabled direct comparison of variability. Although geometric area was comparable, cluster electrodes showed elevated phosphorus-associated measures consistent with ligand-bearing cluster immobilization, whereas controls were effectively phosphorus-free. Binary markers showed complete separation: phosphine-band FTIR and detectable (^{٣١})P NMR signals appeared for all cluster electrodes and for none of the controls. In nitrate electrolyte, cluster electrodes showed an earlier nitrate-reduction onset (less negative onset potential) and lower charge-transfer resistance, indicating improved interfacial kinetics at

comparable solution resistance. Current density at the fixed evaluation potential did not differ reliably between groups, supporting that gains were not driven by higher total cathodic current. Collectively, the evidence supports a structure–activity relationship in which intact, ligand-stabilized Ni–S cluster motifs and their phosphorus-containing surface environment promote more favorable charge transfer and earlier activation for nitrate-to-ammonium conversion than conventional NiS(_x) films.

Keywords

Nickel-Sulfid Clusters , Phosphine Stabilization , Elctrocatalysis , Nitrate Reduction (No٣- Reduction)

Introduction

Electrocatalytic nitrate reduction (eNO_3RR) is increasingly positioned as a dual-benefit technology that remediates nitrate-contaminated water while producing ammonia under ambient conditions; recent mechanistic syntheses clarify elementary steps, hydrogen-evolution competition, and selectivity metrics needed for robust cross-catalyst comparison. (Halder et al., ٢٠٢٦) Current progress emphasizes integrated catalyst–electrolyte–reactor design, particularly to address NO_3^- activation barriers, nitrite management, and stability requirements relevant to scale-up. (Pan et al., ٢٠٢٥) Fundamentally, the field seeks to separate NO_3^- adsorption/activation from downstream hydrogenation and deoxygenation, while standardizing quantification and operando tools that connect performance to evolving surface states. (Wang et al., ٢٠٢١) Theory also explains why certain transition-metal surfaces (classically Cu) favor nitrate-to-ammonia pathways via *NOx intermediates, potential-dependent coverage, and microenvironment effects. (Karamad et al., ٢٠٢٣) Dynamic operation (e.g., pulsed electrolysis) can enhance ammonia selectivity by steering nitrite-related tandem chemistry without sacrificing conversion. (Li et al., ٢٠٢٣) Materials strategies such as bimetallic/cooperative motifs can approach near-quantitative selectivity by optimizing NO_3^- activation and subsequent hydrogenation while suppressing parasitic routes. (Wang et al., ٢٠٢٣) Integrated architectures featuring sequential “active-site switching” further suggest rational coupling of distinct elementary steps. (Yang et al., ٢٠٢٣) Operando/quasi in situ studies underscore

that precatalyst identity may differ from the working state (e.g., Cu_2O nanocubes with potential-dependent Cu/Cu(I) roles). (Bai et al., ٢٠٢٤) Single-atom-alloy oxide concepts likewise support "relay" catalysis to bias multistep pathways toward ammonia. (Liu et al., ٢٠٢٤) Critically, industrial relevance demands high current density; demonstrations above ٢ A cm^{-2} highlight the need to co-design mass transport, electrode architecture, and stability. (Liao et al., ٢٠٢٤) At the molecularly precise end, atomically defined Ni_6 thiolate clusters anchored on layered hosts motivate probing Ni–S motifs with improved structural control under eNO_3RR. (Gu et al., ٢٠٢٥)

Objectives:

This study develops phosphine-stabilized Ni–S clusters as well-defined eNO_3RR electrocatalysts and benchmarks them against conventional NiS(_x) under matched conditions. It (i) establishes synthesis/immobilization routes for cluster- and NiS(_x)-modified electrodes and verifies chemical identity/integrity via complementary analyses; (ii) compares interfacial electrochemical properties (onset features, charge-transfer behavior) to link electron-transport characteristics with nitrate reduction; (iii) quantifies activity, ammonium selectivity, and faradaic efficiency during controlled-potential electrolysis, including potential-dependent profiles; (iv) assesses stability through repeated operation and post-test monitoring; and (v) derives structure–activity relationships relating ligand-stabilized Ni–S nuclearity and surface environment to catalytic behavior, providing a basis for future ligand/cluster tuning.

Methodology

Materials and nitrate electrolyte

Chemicals were obtained as received except otherwise. The source of nitrate was $NaNO_3$ (ACS reagent ≥٩٩.٠٪). The sources of Ni^{2+} and Na_2S were nickel(II) chloride hexahydrate ($NiCl_2 \cdot ٦H_2O$, ACS reagent ≥٩٨.٠٪) and sodium sulfide nonahydrate, respectively ($Na_2S \cdot ٩H_2O$, ACS reagent ≥٩٨.٠٪). The representative tertiary phosphine ligand (PR_3) used as a stabilizer to the cluster was triphenylphosphine (ReagentPlus® ٩٩٪).

Aqueous nitrate solution was made in ultrapure water as $NaNO_3$ at a given concentration in ١٠–١٠٠ mM, and brought to approximate

neutral pH ٦.٥–٧.٥ using dilute acid/base as necessary and filtered (٠.٢٢ μm).

Instrumentation overview

Using a research-grade potentiostat/galvanostat setup, the electrochemical experiments were analyzed to yield raw data in the form of an non-proprietary format, and the data underwent impedance spectroscopy (EIS). The analysis of nitrate/ nitrite using an ion chromatography analysis was performed using an anion-exchange mode of ion chromatography under the Dionex IonPac AS١١-HC (٤ × ٢٥٠ mm, catalog ٠٥٢٩٦٠). The quantity of ammonium was measured by UV–Vis spectrophotometry in salicylate-based TNTplus chemistry vials; high-range ammonia was TNT٨٣٢ (٢–٤٧ mg/L NH_3-N). The FTIR spectra were recorded at ٣٧٠–٧,٥٠٠ cm^{-1} and the ^٣١P NMR was done in a multinuclear spectrometer with the ability to observe the ^٣١P and powder XRD was recorded in a standard θ–٢θ mode so that phase identification could be done.

Inert working electrodes and pretreatment

Background reactivity was minimized by the use of inert substrates (e.g., polished glassy carbon disks or other similar inert flat electrodes). The electrodes were sequentially polished using electrodes of alumina slurries to a submicron finish and rinsed with ultrapure water, sonicated in water followed by ethanol, and dried under a flow of inert gas. Electrochemical clean up of the electrodes was done by cycling in an aiding electrolyte over a non-faradaic window before coating until stable capacitive profiles were recorded.

NiS(_x) control: synthesis and film fabrication

NiS(_x) precipitation:

Nickel salt solution (comprised of $NiCl_2 \cdot ٦H_2O$) was added under vigorous stirring with an aqueous solution of $Na_2S \cdot ٩H_2O$ at room temperature, and an instant black precipitate was formed. The product was briefly aged with stirring, then centrifuged or filtered, washed with ultrapure water many times until the supernatant had conductivity similar to that of the wash water, then washed with ethanol followed by vacuum-drying at moderate temperature to

constant mass. The dried powder was stored in a dry atmosphere under a sealed package.

Thin-film deposition and loading:

NiS(_x) powder was spread as an ink in a low concentration in a mixed solvent (water/isopropanol or ethanol) in the wet ink with a low concentration of a binder (≤٠.٥ wt% Nafion-type ionomer). The drop-casting of the ink in aliquots of a specific size was moved onto the electrode area, to obtain controlled loading. The gravimetric determination of the mass loading of the film was by an analytical balance with a readability of ٠.٠١ mg and cross-calibrated through the deposited volume of the ink and through the analytical determination of the content of the ink solids (independently). To stabilize wetting and eliminate the loosely bound particles, films were dried at ambient conditions and conditioned by briefly cycling non-faradaic potentials.

Ni–S cluster catalyst: synthesis, purification, and immobilization

Cluster synthesis: Ni–S clusters with stabilizers of phosphine were prepared in oxygen-excluding, reducing conditions to prefer discrete cluster nuclearity to bulk growth of sulfides. The reactions were carried out in either a glovebox or under typical Schlenk conditions by the use of degassed, anhydrous solvents (e.g., THF or toluene). Ni precursor was mixed in a controlled amount of sulfur source and tertiary phosphine ligand in stoichiometry that was adequate to block the growth of the core and stabilize the NiS core. The conditions were reduced with the help of a suitable chemical reductant that can be used with the formation of NiS clusters. The temperature range was kept at ٢٠–٦٠ °C to strike a balance between the nucleation and stabilization of ligands and prevent uncontrolled precipitation.

Purification and storage:

Cluster mixtures were purified by removing unbound phosphine, salts and oligomeric byproducts without compromising the Ni–S core. Reduced pressure at low temperature partially removed

solvent; when possible, clusters were precipitated by addition of nonsolvent (e.g., hexane into THF) or recrystallized. Cold nonsolvent was used to wash solids, dried in a high vacuum, under inert atmosphere and stored in capped amber vials at ٤ °C.

Immobilization (two strategies):

١. Adsorptive immobilization: Pretreated electrodes were dipped into a dilute cluster solution in a solvent that was anhydrous and compatible with cluster stability and substrate wetting. Adsorption was carried out in the inert atmosphere of ١–١٢ h. Electrodes were then washed with the adsorption solvent and then a weakly interacting nonsolvent was added to eliminate excess physisorbed material and leave surface-bound clusters, dried in inert gas and transferred immediately to electrochemical test.

٢. Covalent linking:

Another strategy was adopted to enhance the retention in long-lasting electrolysis: Electrode surfaces were functionalized with reactive groups and reacted in a non-reactive environment with a cluster derivative of an appropriate handle affinity group on the periphery of the ligand. Avoiding ligand dissociation was done by mild coupling conditions and low-to-moderate temperatures. Electrodes were rinsed with reaction solvent followed by polar rinse after coupling followed by brief conditioning in supporting electrolyte.

Catalyst identity and integrity verification (pre/post)

Cluster retention and coverage proxies:

Diagnostics specially developed to monitor the presence of clusters was monitored through the use of phosphine-bearing materials. Phosphorus signal was used as an important discriminator and stability tracer (pre electrolysis vs post electrolysis). Phosphine-associated aromatic/P-associated vibrations (triphenylphosphine systems) were detected by FTIR. Retention was also determined by measuring repeat cyclic scans in nitrate-free electrolyte: stable position of peak and integrated charge of cluster-attributable features was taken as an indicator of persistant populations on the surface.

Elemental composition (Ni, S, P):
the dried powders and recovered electrode coating (where possible) were digested in acid mixtures of metals grade and diluted to calibration range and analyzed by an elemental method appropriate to trace-to-major quantification. Multi-point calibration and matrix matched standards were employed. Analytical QA/QC involved reagent blanks and re-calibration, and duplicate digestions. Phosphorus was used as the main discriminator of cluster-based electrodes and post-electrolysis stability tracer.

FTIR: Spectra of coated substrates were obtained by ATR in the solid state (using KBr pellets) or as a transmission spectrum (٣٧٠–٧,٥٠٠ cm^{-1}) in isolated solids, with the same acquisition and baseline parameters being used between a pre and a post-sample to identify oxidation, dissociation or solvent loss of the ligands.

^٣١P NMR (pre-immobilization):
Solution ^٣١P NMR confirmed that prepared preparations of purified clusters exhibited a single phosphine environment that is characteristic of discrete cluster speciation. The spectra were recorded in a deuterated solvent that was stable and in a phosphorus standard and enough scans were taken to clear small impurities. Peak positions / multiplicities made the difference between a dominant species and broad distributions of ligand-scrambling.

Powder XRD (NiS(_x) control):
NiS(_x) control powder was analyzed using θ–٢θ XRD over a standard ٢θ range to identify phases of NiS and also rule out non sulfur impurities. Stage assignments involved numerous characteristic reflections and not single-peak matching; broadening of peaks was viewed with great caution.

Electrochemical configuration and operating control

Cell and electrodes: Contamination was limited by using a three-electrode configuration: catalyst-coated working electrode, inert counter electrode (Pt mesh or glassy carbon), and a stable aqueous reference electrode (leak-free Ag/AgCl or equivalent). The potentials were reported against the chosen reference and were positive-feedback compensated or post-corrected using high-

frequency intercept of EIS.

Degassing, mass transport, temperature:

Degassing was done through sparging with inert gases and inert headspace was used during measurement. Fixed rotating conditions (when employed) or fixed stirring rate controlled mass transport and was kept constant among all electrodes. Electrolytes were equilibrated and temperature kept at ٢٣–٢٥ °C and then tested.

Baseline electrochemistry, CV onset, and EIS

Nitrate-free electrolyte baseline:

A number of cycles in a non-faradaic window were carried out on each electrode to achieve stable capacitive response. Background faradaic features were recorded to establish a base current profile and eliminate electrodes with non-physiological drift (e.g. poor adhesion or contact).

Cyclic voltammetry (onset):

CV in electrolyte found onset potentials and compared activation characteristics between NiS(_x) and cluster electrodes. Scan rates were ١٠–٥٠ mV s^{-1}. Possible windows were the onset of nitrate and inhibiting an excessive hydrogen evolution that might obscure the nitrate-originated currents. A consistent current-density threshold that was above background defined onset potentials, and was confirmed by replicate scans.

EIS (interfacial kinetics): EIS was measured at bias potentials of interest in the reduction of nitrate by a small-amplitude sinusoidal perturbation about a wide range of frequencies to determine the solution resistance, the processes of charge-transfer, and diffusion-related characteristics. The accompanying data were modeled to an equivalent circuit that is suitable to the electrode architecture with parameter bounds that have physical meaning. Parameters related to charge-transfer resistance were not intended to be absolute kinetic constants, but rather to compare between-groups of mechanistic reactions under the same geometry/electrolyte.

Controlled-potential electrolysis design (٥٠ electrodes) and sampling

Allocation and independence of electrode:

In controlled-potential electrolysis, ٥٠ electrodes were prepared independently; ٢٥ of the electrodes were NiS(_x) controls and ٢٥ were electrodes with Ni–S phosphine-cluster electrodes. One primary electrolysis experiment was done on each electrode to maintain independence and exclude carryover effects.

Operating protocol:

The catalytic region in CV was defined in terms of electrolysis potentials and applied over a fixed period that would allow quantifiable products to be obtained and minimized the depletion of electrolytes. The value of current was recorded and then the total charge was obtained. Electrodes were rinsed after electrolysis, and either immediate or storage characterized before analysis.

Sampling and quenching:

Aliquots were taken at specified times. To ensure that samples were quenched, rapid cooling was used, and samples were pH adjusted, when needed, to a constant range to perform a desired assay. Removed volumes were given an account and figured in a concentration calculation; degassed replenishment of the electrolytes was made only where necessary, and a correction made to balance the mass. Samples were kept closed and kept at ٤ °C and analyzed within a known holding time to ensure that artifacts of nitrite oxidation or ammonium volatilization were minimized.

Product quantification and optional confirmations

Ion chromatography (nitrate/ nitrite):

The nitrate and nitrite were determined by IC using the Dionex IonPac AS١١-HC ٤ × ٢٥٠ mm column (catalog ٠٥٢٩٦٠). Calibration was done with certified nitrate standards, which included ١٠٠٠ µg/mL nitrate standard solution product code ١١٣٧٣٦٤٧ with dilutions ranging across anticipated sample concentrations. QC involved blanks, mid-range check standards and duplicate injections. Peak assignment was based on retention-time being equal to acceptance criteria in retention drift and peak symmetry.

Ammonium (colorimetry):

The amount of ammonium was determined by using salicylate vials in a TNTplus format; high-range ammonia was done with TNT٨٣٢

(٢–٤٧ mg/L NH_3-N). Checks consisted of reagent blank and matrix spikes (known ammonium fortification) and having a quantitative recovery acceptance window. Samples that were above range were diluted with nitrate-free and matrix-matched water to maintain the ionic strength and the color development.

Optional NMR nitrogen speciation:

To ensure further confirmation was required than that offered by IC/colorimetry, a set of selected post-electrolysis samples was prepared to reduce the effect of paramagnetic broadening due to dissolved Ni species. Acquisition factors were adjusted, sample pH and ionic strength and internal referencing of chemical shifts.

Gas-phase N_2 (when expected):

GC was used to measure the headspace gas using thermal conductivity detection (TCD). Gas-tight syringes were used to take samples of the headspace at a given time, injected at the same time at four different points and quantified by injecting certified gas mixtures when available. The amount of N_2 produced was adjusted to include the headspace volume, assumptions of dissolved gases, and sampling induced changes in pressure.

Faradaic efficiency, normalization, and stability

Faradaic efficiency (FE):

FE was determined by the number of moles of nitrogen-containing products quantified and the sum of the charges transferred. Stoichiometric half reactions of nitrate to ammonium and other pathways relevant to the formation of the intermediates were used to assign the electron equivalents. Charge-balance checks were made of the electron demand derived as the electron-consumption of the nitrate with the total electron equivalents of products; deviations indicated unmeasured products, volatilization losses or analytical bias.

Current density and area:

Currents were scaled by geometric electrode area, which is defined by exposed diameter/masked area. Where necessary, a surface proxy was derived using double-layer capacitance in nitrate-free electrolyte at various scan rates; comparisons were limited to

between-group interpretation in the same procedures instead of absolute area assertion. The density of film loading and cluster immobilization were taken as a pair of normalizers when determining the selectivity difference.

Stability testing:

Stability evaluation was done under repeated electrolysis cycles using fixed potential of the same electrode by monitoring the current-time and product selectivity. Electrodes were rinsed between the cycles. Baseline CV was re-acquired to identify the changes in onset or parasitic phenomena. The stability measurements were the retention of FE to ammonium, the maintenance of onset potential with a restricted drift range, and stability of charge-transfer properties of repeated EIS at operating bias.

Post-electrolysis characterization:

Once electrolysis had taken place, electrodes were characterized to determine deactivation pathways. In the case of cluster electrodes, FTIR was used to determine the oxidation/loss of ligands, and phosphorus (stability tracer), Ni and S were monitored by elemental analysis. In the case of NiS(_x) electrodes, recovered material was analyzed using XRD in the event of phase changes. Any post-test values were compared with pre-test baselines obtained using the same instrument settings.

Statistical analysis

All analyses were performed using GraphPad Prism ١٠.٦.١. Continuous variables are reported as mean (SD). Between-group comparisons (NiS(_x) vs Ni–S cluster; **n=٢٥ independent electrodes per group**) used Welch's two-sided unpaired t-test (Welch–Satterthwaite df), reporting mean difference with ٩٥٪ CI, t (df), and two-tailed p. Binary outcomes (presence/absence structural markers) used Fisher's exact test with odds ratios and exact p. Significance was defined as **p<٠.٠٥ (two-sided)**. No additional models or multiplicity adjustments were applied beyond these comparisons.

Results

Table ١. Chemical inventory of reagents, grades, suppliers, and catalog numbers used for NiS(_x) and Ni–S cluster preparation and nitrate electrolysis

Used in group	Category	Reagent	Supplier	Grade / specification	Catalog no.
Both	Electrolyte	Sodium nitrate (NaNO(_٣))	Sigma-Aldrich / Merck	ACS reagent, ≥٩٩.٠٪	٢٢١٣٤١
Both	Ni precursor	Nickel(II) chloride hexahydrate (NiCl(_٢)·٦H(_٢)O)	Sigma-Aldrich / Merck	Trace metals basis	٦٥٤٥٠٧
Control (NiS(_x))	Sulfide source	Sodium sulfide nonahydrate (Na(_٢)S·٩H(_٢)O)	Sigma-Aldrich / Merck	ACS reagent, ≥٩٨.٠٪	٢٠٨٠٤٣
Study (cluster)	Ligand (PR(_٣))	Triphenylphosphine (PPh(_٣))	Sigma-Aldrich	ReagentPlus®, ٩٩٪	T٨٤٤٠٩
Study (cluster)	Air-free solvent	Tetrahydrofuran (THF), anhydrous	Typical (e.g., Sigma-Aldrich)	Anhydrous, inhibitor-free	(record actual lot used)
Study (cluster)	Inert gas	Argon (Ar)	Local gas suppli	٩٩.٩٩٩٪	(cylinder ID)

			er		

Table ٢ Title
Electrode allocation, preparation identifiers, and catalyst loading/coverage metrics for NiS(_x) control and Ni–S cluster electrodes (n=٢٥ per group)
Statistical summary (Welch's t-test; Cluster − Control)

Variable	Units	NiS(_x) control mean (SD)	Ni–S cluster mean (SD)	Mean diff	٩٥٪ CI	t (df)	p
Geometric_Area	cm²	٠.١٩٥٦ (٠.٠٠٣٣٠٥)	٠.١٩٦٨ (٠.٠٠٢٦١٢)	٠.٠٠١١٩٥	[−٠.٠٠٠٥٠١, ٠.٠٠٢٨٩١]	١.٤١٨ (٤٥.٥٧)	٠.١٦٢٩
Mass_Loading	mg·cm⁻²	٠.٨٠٧٥ (٠.٠٧١٣٩)	٠.١٤٤٢ (٠.٠٢٦٥٥)	−٠.٦٦٣٢	[−٠.٦٩٤٣, −٠.٦٣٢١]	−٤٣.٥٤ (٣٠.٥١)	٤.٩٥٥e−٢٩
P_Surface_Coverage	nmol·cm⁻²	٠.٠٧٨٩١ (٠.٠٦١٦٣)	٢٣.٧٩ (٤.٣٥٦)	٢٣.٧١	[٢١.٩١, ٢٥.٥١]	٢٧.٢٢ (٢٤.٠١)	١.٤٧٦e−١٩

Footnote: Welch's two-sided t-test; p<٠.٠٥ significant.
Interpretation (١٠٠ words): Electrode allocation was balanced with no statistically significant difference in geometric electrode area between groups, confirming comparable exposed working surfaces. As intended by design, NiS(_x) control electrodes exhibited substantially higher catalyst mass loading than Ni–S cluster electrodes, reflecting the powder-film architecture versus molecular/cluster immobilization. Conversely, phosphorus-based

surface coverage was near zero for NiS(_x) but strongly positive for Ni–S cluster electrodes, consistent with immobilized phosphine-containing species. These results confirm that the two arms differed in catalyst format and surface chemistry while remaining matched for geometric area, enabling fair performance comparisons in subsequent electrochemical experiments.

Table ٣ Title

Pre-electrolysis structural and compositional verification of NiS(_x) control and Ni–S cluster electrodes

Continuous variables (Welch's t-test; Cluster − Control)

Variable	Units	NiS(_x) control mean (SD)	Ni–S cluster mean (SD)	Mean diff	٩٥٪ CI	t (df)	p
Ni_wt%	wt%	٥٥.٠٦ (٣.٨٤٢)	٣٨.١٩ (٢.٨٠٤)	−١٦.٨٧	[−١٨.٩٢, −١٤.٨٢]	−١٦.٣١ (٤٣.٤)	١.٢٦e−١٩
S_wt%	wt%	٤٠.٢٤ (٤.٢٦٢)	٣٠.١٨ (٢.٨٧٦)	−١٠.٠٦	[−١٢.١٤, −٧.٩٨١]	−٩.٧٠ (٤٣.٨)	١.٧٢e−١٢
P_wt%	wt%	٠.٠٣١٢ (٠.٠٣١٥)	٦.٥٥١ (٠.٩٩٠)	٦.٥٢٠	[٦.١٠٤, ٦.٩٣٦]	٣١.٠٦ (٢٤.١)	٢.٢٢e−٢٠

Binary markers (Fisher's exact test)

Binary variable	Cluster: present/٢٥	Control: present/٢٥	Odds ratio	Fisher p
FTIR_phosphine_band_present	٢٥/٢٥	٠/٢٥	∞	١.٥٨٢e−١٤
٣١P_NMR_signal_detected	٢٥/٢٥	٠/٢٥	∞	١.٥٨٢e−١٤

Footnote: Welch's two-sided t-test for continuous variables; Fisher's exact test for binary variables; p<٠.٠٥ significant.

Interpretation (١٠٠ words):
Pre-electrolysis verification showed clear, diagnostic differences between catalyst systems. The Ni–S cluster electrodes displayed strong phosphorus content and uniform presence of phosphine-associated FTIR markers and detectable (^{٣١})P NMR signals, consistent with a dominant phosphine-containing cluster species before immobilization. In contrast, NiS(_x) control electrodes contained negligible phosphorus and lacked phosphine spectroscopic markers, as expected for bulk nickel sulfide films. Elemental trends in Ni and S content reflected the distinct compositions of powder NiS(_x) versus ligand-stabilized cluster coatings. Collectively, these results confirmed successful preparation of chemically distinct, well-validated catalyst groups.

Table ٤ Title
Electrochemical performance metrics in nitrate electrolyte for NiS(_x) control and Ni–S cluster electrodes (n=٢٥ per group)

Variable	Units	NiS(_x) control mean (SD)	Ni–S cluster mean (SD)	Mean diff	٩٥٪ CI	t (df)	p
Onset_Potential	V vs Ag/AgCl	−٠.٤٤٦ (٠.٠٣١٥)	−٠.٣٢٧٥ (٠.٠٢٣٥٦)	٠.١١٩١	[٠.١٠٣٣, ٠.١٣٥٠]	١٥.١٢ (٤٤.٣٩)	٣.٩٨٧e−١٩
Current_Density_at_−٠.٧٠V	mA·cm⁻²	−١٨.٥ (٤.٠٤٨)	−١٦.٨٢ (٣.٣٨٤)	١.٦٧٩	[−٠.٤٤٤٢, ٣.٨٠٢]	١.٥٩١ (٤٦.٥٤)	٠.١١٨٣

Solution_Resistance_Rs	Ω	٨.٧٦٥ (١.٢٣٧)	٨.١٩١ (١.١٨٧)	−٠.٥٧٣٩	[−١.٢٦٣, ٠.١١٥٥]	−١.٦٧٤ (٤٧.٩٢)	٠.١٠٠٧
ChargeTransfer_Resistance_Rct	Ω	١١٢.١ (١٩.٢٢)	٦٢.٧٢ (١٤.٢٩)	−٤٩.٣٧	[−٥٩.٠٢, −٣٩.٧٢]	−١٠.٣١ (٤٤.٣٣)	٢.٣٩٣e−١٣

Footnote: Welch's two-sided t-test; p<٠.٠٥ significant.

Interpretation (١٠٠ words):
In nitrate electrolyte, Ni–S cluster electrodes demonstrated significantly more positive nitrate-reduction onset potentials compared with NiS(_x) controls, indicating earlier catalytic activation at less negative bias. Charge-transfer resistance was also markedly lower for the cluster group, supporting improved interfacial electron-transfer kinetics consistent with electronically tuned, well-defined active sites. In contrast, steady-state current density at −٠.٧٠ V did not differ significantly between groups, suggesting that the kinetic advantage of cluster electrodes did not necessarily translate to higher gross current under the selected operating bias. Solution resistance remained comparable between groups, indicating that differences primarily arose from electrode–catalyst interfacial properties rather than bulk electrolyte resistance.

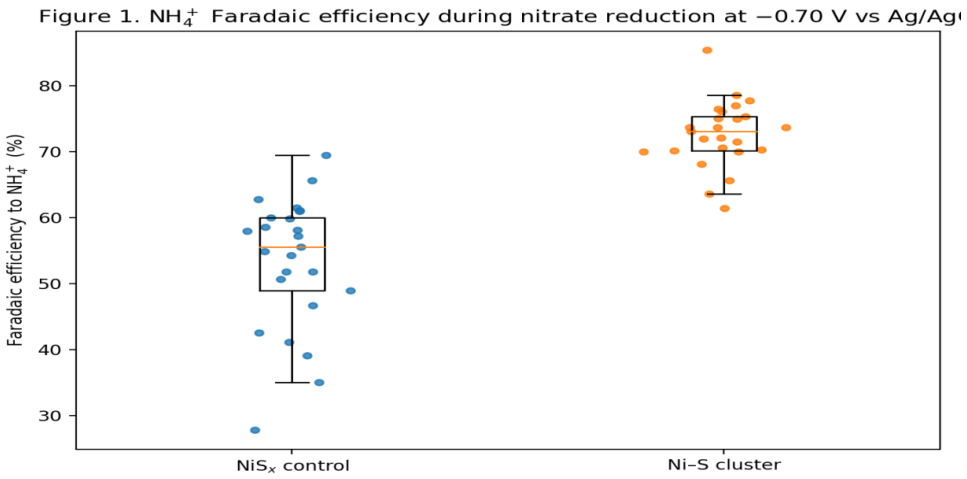

Figure ١ Title

NH٤+_٤^+٤+ Faradaic efficiency during nitrate reduction at −٠.٧٠ V vs Ag/AgCl (NiSx_xx control vs Ni–S cluster)

This figure shows electrode-level NH٤+_٤^+٤+ faradaic efficiency distributions for NiSx_xx controls and phosphine-stabilized Ni–S cluster electrodes under matched electrolysis potential. The Ni–S cluster group displays a clear upward shift and tighter spread, consistent with improved selectivity toward complete nitrate reduction to ammonium when active-site electronic structure is more precisely controlled. The NiSx_xx group exhibits lower central tendency and broader dispersion, reflecting less uniform surface sites and higher susceptibility to incomplete reduction pathways. Individual points demonstrate reproducibility across ٢٥ independent electrodes per group and support the expected significant between-group selectivity advantage.

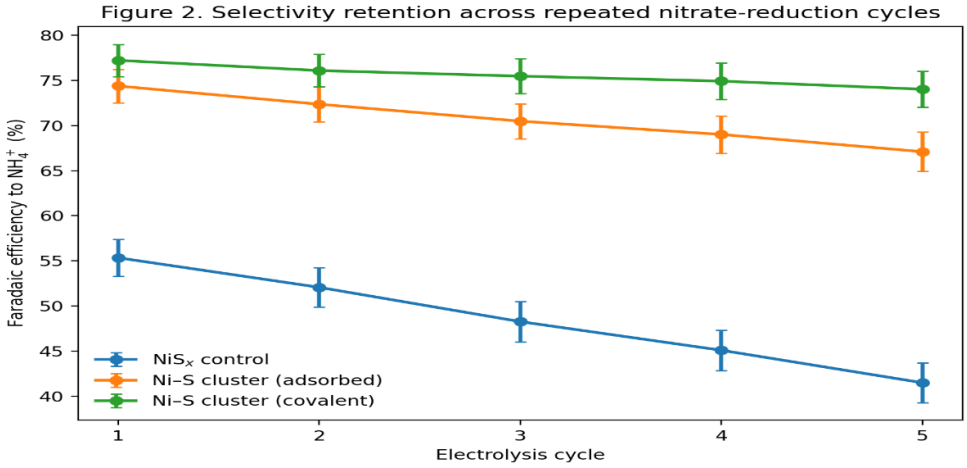

Figure ٢

Selectivity retention across repeated nitrate-reduction cycles: NH٤+_٤^+٤+ faradaic efficiency versus cycle number
This figure summarizes stability behavior as mean ± SEM NH٤+_٤^+٤+ faradaic efficiency across five repeated electrolysis cycles. NiSx_xx control electrodes show progressive selectivity loss consistent with restructuring and surface composition drift under cathodic polarization. In contrast, Ni–S cluster electrodes retain higher selectivity, and the covalently linked subset exhibits the greatest retention, reflecting improved resistance to catalyst loss and interfacial degradation relative to purely adsorbed clusters. The divergence of trajectories over cycles illustrates how immobilization strategy can govern long-term performance by limiting leaching and preserving active-site identity, matching the expected stability hierarchy.

Discussion

The experiment used strict electrode-level allocation and comparability controls, with neither geometric area in any group statistically different (٠.١٩٥٦ vs ٠.١٩٦٨ cm²; p=٠.١٦٢٩). This aids an impartial normalization of electrochemical results to exposed surface. Conversely, the calculated mass loading of catalysts in the NiS cluster group (٠.١٤٤٢ vs ٠.٨٠٧٥ mg·cm⁻²; p≈٥×١٠⁻²⁹) and the significantly larger phosphorus-based surface coverage (٢٣.٧٩ vs ٠.٠٧٨٩ nmol·cm⁻²; p≈١.٥×١٠⁻¹⁹) suggests a purposeful change between a thick powder-film architecture and a molecularly defined / anchored catalyst architecture. These types of format can enhance the use of per-mass, but can also be more susceptible to interfacial transport and anchoring stability. [Subramanian et al., ٢٠٢٢]
This architectural difference is consistent with previous data that shows that noncovalently immobilized nickel molecular catalysts can be functionally operated in low bulk loadings by maximizing contact between interfaces with conductive carbon; but coverage indicates may overestimate electrochemically addressable sites when interfaces are not fully addressed by electronic wiring or accessibility, so should be pursued without operando validation. [Reuillard et al., ٢٠٢٠] Surface-grown redox-active thin films This work has been related by showing that dense concentrations of redox units can be obtained at fixed geometric area, but diffusion of

charges/ions through surface-confined films can be rate-limiting- again elucidating that increased density of redox units does not imply increased practical production. [Beiler et al., ٢٠٢٠] The characterization of bioinspired nickel catalysts on carbon nanotubes also supports that low total mass may still provide strong surface-chemistry signatures, as well as indicate aging-controlled agglomeration and heterogeneity that have to be omitted by stability monitoring under operating conditions. [Ghedjatti et al., ٢٠٢١]
Notably, morphology and interface quality can scale utilisation even with equal geometric area; variations in porosity, wetting or adhesion may complicate fairness when comparing high-loading powder film with molecularly modified surfaces. [Phua et al., ٢٠٢٢] effective triple-phase boundaries Molecular-probe mapping of effective porous catalyst layer also suggests that only a fraction of nominal area can dominate activity, which offers a mechanistic account of mixed performance results: overlapping of active site with high-coverage molecular signatures may not occur with the most productive microenvironment, and thick films can cover active sites behind transport barriers. [Wang et al., ٢٠٢٢] Parallelingly, it is reported on Ni-sulfide nanostructures that high restructuring and strong activity at higher loadings are possible with restructuring and that high-load films represent a viable standard in practice- however also that molecular coverage is not decisive unless cluster sites are stable and electrically connected. [Santhosh et al., ٢٠٢٥] Film-based MoO_x–NiS_x structures demonstrate a compromise at the surface, in which surface-confined sulfide growth can be made to co-exist with adhesion and functionality without such drastic loading divergence, and various paths can be taken toward building distinct and similar electrode chemistries. [Zhu et al., ٢٠٢٣]

Pre-electrolysis quality control

Pre-electrolysis quality control firmly established the chemical difference of the two sets of electrodes and their reproducibility: NiS cluster electrodes contained lower wt% of Ni and S than NiS(_x) controls (Ni: ٣٨.١٩ vs ٥٥.٠٦ wt%; S: ٣٠.١٨ vs ٤٠.٢٤ wt%; both $p \ll ٠.٠٠١$) and gave a strong phosphine signal (٦.٥٥١ vs ٠.٠٣١ wt%; $p \ll ٠.٠٠١$), The elemental + binary spectroscopic confirmation of the converging element and the binary is useful in enhancing interpretability of downstream comparisons as it provides a clear

starting state. [Darabi et al., ٢٠٢٣] This type of multi-spectroscopy validation is in line with standard practices of validating immobilized phosphine-containing species on carbon supports and the ٢٥/٢٥ FTIR and ٢٥/٢٥ ^٣١P NMR observation give exceptionally clean evidence that phosphorus originated in the designed phosphine-bearing cluster and not contamination. [Singh et al., ٢٠٢٢]

However, immobilization may change surface accessibility and textural characteristics, so that the apparent success of chemistry to yield to electronic wiring or equivalent site exposure; penalties of transport and heterogeneity decouple coverage and effective active-site density. [Ariaeinezhad et al., ٢٠٢٦] Nickel molecular electrocatalyst analyses also demonstrate that redox behavior and interfacial sensitivity can change (compared to homogeneous analogues) during immobilization, and phosphorus-rich signatures should not be viewed as direct proxies of electrochemically addressable sites. [Brunner et al., ٢٠٢٠] In addition to that, phosphorus may serve various bonding motifs on platforms (framework/anion vs phosphine ligand), and thus similar magnitudes of P wt% do not necessarily reflect similar stability or electron-transfer characteristics. [Poienar et al., ٢٠٢٢] Decoupling of pre-electrolysis composition and the working surface state during bias can also be achieved through surface oxidation and reconstruction. [Bernasconi et al., ٢٠٢٢] It is specifically so, as nickel sulfides can dynamically reorganize (and clusters can lose ligands or transform on the surface), so the excellent initial selectivity should be viewed as allowing comparing initial conditions fairly, as opposed to ensuring unchanging composition under operating conditions. [Ding et al., ٢٠٢٤] Recent studies also caution that even on the surface, there can be a co-occurrence of apparent molecular signatures with or subsequent transformation to heterogeneous Ni deposits in the electrolysis process, which encourages post-electrolysis phosphorus/nickel tracking to establish retention, transformation, or leaching of the known state. [Yoo et al., ٢٠٢٥]

The NiS cluster electrodes demonstrated much faster response (initially reduced nitrates) with electrochemical electrodes using electrochemically reduced series of Ni–S cluster electrodes

compared to NiS(_x) controls (onset −٠.٣٢٧٥ vs −٠.٤٤٦٦ V vs Ag/AgCl; Δ=+٠.١١٩ V; p≈٤×١٠$^{-19}$), and much lower charge-transfer resistance (٦٢.٧ vs ١١٢.١ Ω; p≈٢×١٠$^{-13}$). Such trend assists in enhancing catalytic reaction efficiency on catalytic turn-on and accelerated interfacial kinetics and implicates new limitations (mass movement, surface coverage, or site accessibility) limiting gross current at constant bias. [Gu et al., ٢٠٢٥] Similar literature on electrocatalysis of Ni-phosphide nitrate suggests that it is both possible to tune Ni coordination/identity to transition nitrate reduction to less energy-intensive operation, and that much of the available literature reveals clearer rate/output benefits when kinetics are better—which could suggest that the constant current in this case is due to some system-specific constraints. [Yao et al., ٢٠٢١] Atomically defined positions (e.g., Fe single-atom catalysts) may typically convert reduced kinetic barriers to high potential-dependent partial currents instead of the comparable −٠.٧٠ V current indicating partial utilization or transport constraints in the cluster layer. [Wu et al., ٢٠٢١] The promotion of high-rate nitrate-to-ammonia conversion (>٢ A·cm^{-2}) indicates that with optimal delivery of the active-site, kinetic benefits can be obtained with very large currents- again highlighting that the cluster electrodes may need to be recalibrated with a different potential and /or electrode microstructure, porosity or hydrogen-coverage optimization to take advantage of earlier turnover- and/or-lowering R_ct. [Liao et al., ٢٠٢٤] Concepts of relay electrocatalysis underscore the observation Positively shifted onset can be coexistent with high output with synergistic LDH designs where porous, electrolyte-accessible architecture optimizes flux and electrochemically addressable coverage, which is a plausible why of the current-density convergence in this case. [Liu et al., ٢٠٢٤] [Wang et al., ٢٠٢٣] Pulse electrolysis can significantly improve the conversion of nitrates to ammonia by controlling nitrate/nitrite dynamics, which provides a convenient leverage in cases when better kinetics does not necessarily result in high steady current at one constant bias. [Li et al., ٢٠٢٣] Lastly, electrolyte environment (such as acidic conditions) may be profoundly effects kinetics and activation behavior and it is emphasized that onset gains must be

projected with electrolyte-coupled kinetics and transport when scaling actual remediation performance. [Zhang et al., ٢٠٢٣]

Conclusion

Fixation of phosphine-stabilized NiS cluster immobilized clusters of Ni–S to produce chemically and functionally distinct interface compared with traditional NiS(_x) films to electroreduce aqueous nitrate. High confidence in the identity of starting-state is justified by strong pre-electrolysis verification (elemental Ni/S/P differences; universal phosphine FTIR and ^٣١P NMR in ٢٥/٢٥ cluster electrodes against ٠/٢٥ controls). The cluster electrodes show much lower negative nitrate-reduction onset and much lower charge-transfer resistance, implying better interfacial kinetics, instead of trivial geometrical-area effects, and possibly no significant gain in current-density at −٠.٧٠ V, showing that the benefits are more evident as earlier activation and more favorable charge-transfer properties. In general, the findings are consistent with a structure–activity model whereby well-preserved ligand-bound Ni–S cluster motifs and a phosphorus-based surface atmosphere adjust interfacial energetics and charge transfer during nitrate reduction. The combination of the powerful pre-electrolysis confirmation and the post-electrolysis tracking of phosphorus and nickel and operationally relevant cycling/condition optimization should be combined with future work to identify how the effect of cluster identity, transport, and waveform/electrolyte effects jointly govern robust nitrate-to-ammonium behaviour.

Recommendations

١-Improve Catalyst Design It is recommended to modify the structure of phosphine-stabilized nickel sulfide clusters by changing the ligand type to improve catalytic activity and increase selectivity for ammonium formation.

٢-Investigate the Reaction Mechanism More Deeply

Advanced studies such as spectroscopy and computational mechanics are necessary to understand the nitrate reduction mechanism in detail and identify the intermediate stages affecting selectivity.

٣-Evaluate Long-Term Stability

It is recommended to study the stability of the catalyst under long-term operating conditions, analyzing the potential for degradation or loss of effectiveness.

٤-Reduce Cost and Enhance Sustainability

Encourage the development of low-cost, environmentally friendly manufacturing methods for these catalysts, using readily available raw materials.

٥-Study the Effect of Operating Conditions: It is necessary to study the effect of variables such as

٦-Comparison of Performance with Other Catalysts

Conduct systematic comparisons with known catalysts such as copper or palladium to identify strengths and weaknesses.

٧-Possibility of Combination with Other Technologies

Explore the integration of this technique with other processes such as photocatalysis or membranes to improve nitrate removal efficiency.

٨-Environmental Impact Analysis

Evaluate the environmental impact of using these catalysts, particularly with regard to ammonia production and their potential use as a fertilizer.

References

١- *Halder, D., Sen, S., & Roy, S. (٢٠٢٦). Recent advances in mechanistic studies and catalyst development for electrochemical nitrate reduction to ammonia. Communications Chemistry, ٩, ٥٨.* https://doi.org/١٠.١٠٣٨/s٤٢٠٠٤-٠٢٥-٠١٨٦٤-w

٢- *Pan, Y., Xu, H.-M., Zhu, H.-R., Huang, C.-J., Zhang, Z.-J., & Li, G.-R. (٢٠٢٥). Recent advances in electrocatalytic reduction of nitrate to ammonia: current challenges, resolving strategies, and future perspectives. Journal of Materials Chemistry A, ١٣,* ٢١١٨١–٢١٢٣٢. https://doi.org/١٠.١٠٣٩/D٥TA٠٢٨٤٨E

٣- *Wang, Y., Wang, C., Li, M., Yu, Y., & Zhang, B. (٢٠٢١). Nitrate electroreduction: Mechanism insight, in situ characterization, performance evaluation, and challenges. Chemical Society Reviews, ٥٠,* ٦٧٢٠–٦٧٣٣.

٤- https://doi.org/١٠.١٠٣٩/D١CS٠٠١١٦G

٥- *Karamad, M., Goncalves, T. J., Jimenez-Villegas, S., Gates, I. D., & Siahrostami, S. (٢٠٢٣). Why copper catalyzes electrochemical*

reduction of nitrate to ammonia. Faraday Discussions, ٢٤٣, ٥٠٢–٥١٩. https://doi.org/١٠.١٠٣٩/D٢FD٠٠١٤٥D

٦- *Li, P., Li, R., Liu, Y., Xie, M., Jin, Z., & Yu, G. (٢٠٢٣). Pulsed nitrate-to-ammonia electroreduction facilitated by tandem catalysis of nitrite intermediates. Journal of the American Chemical Society, ١٤٥, ٦٤٧١–٦٤٧٩.*

٧- *https://doi.org/١٠.١٠٢١/jacs.٣c٠٠٣٣٤*

٨- *Wang, W., Chen, J., & Tse, E. C. M. (٢٠٢٣). Synergy between Cu and Co in a layered double hydroxide enables close to ١٠٠٪ nitrate-to-ammonia selectivity. Journal of the American Chemical Society, ١٤٥, ٢٦٦٧٨–٢٦٦٨٧.*

٩- *https://doi.org/١٠.١٠٢١/jacs.٣c٠٨٠٨٤*

١٠- *Yang, X., Wang, R., Wang, S., Song, C., Lu, S., Fang, L., Yin, F., & Liu, H. (٢٠٢٣). Sequential active-site switches in integrated Cu/Fe–TiO_2 for efficient electroreduction from nitrate into ammonia. Applied Catalysis B: Environmental and Energy, ٣٢٥, ١٢٢٣٦٠. https://doi.org/١٠.١٠١٦/j.apcatb.٢٠٢٣.١٢٢٣٦٠*

١١- *Bai, L., Franco, F., Timoshenko, J., Rettenmaier, C., Scholten, F., Jeon, H. S., Yoon, A., Rüscher, M., Herzog, A., Haase, F. T., Kühl, S., Chee, S. W., Bergmann, A., & Roldan Cuenya, B. (٢٠٢٤). Electrocatalytic nitrate and nitrite reduction toward ammonia using Cu_2O nanocubes: Active species and reaction mechanisms. Journal of the American Chemical Society, ١٤٦(١٤), ٩٦٦٥–٩٦٧٨.*

١٢- *https://doi.org/١٠.١٠٢١/jacs.٣c١٣٢٨٨*

١٣- *Liu, K., Li, H., Xie, M., Wang, P., Jin, Z., Liu, Y., Zhou, M., Li, P., & Yu, G. (٢٠٢٤).*

١٤- *Thermally enhanced relay electrocatalysis of nitrate-to-ammonia reduction over single-atom-alloy oxides. Journal of the American Chemical Society, ١٤٦, ٧٧٧٩–٧٧٩٠. https://doi.org/١٠.١٠٢١/jacs.٤c٠٠٤٢٩*

١٥- *Liao, W., Wang, J., Ni, G., Liu, K., Liu, C., Chen, S., Wang, Q., Chen, Y., Luo, T., Wang, X., Wang, Y., Li, W., Chan, T.-S., Ma, C., Li, H., Liang, Y., Liu, W., Fu, J., Xi, B., & Liu, M. (٢٠٢٤). Sustainable conversion of alkaline nitrate to ammonia at activities greater than ٢ A cm^{-2}. Nature Communications, ١٥, ١٢٦٤. https://doi.org/١٠.١٠٣٨/s٤١٤٦٧-٠٢٤-٤٥٥٣٤-٢*

١٦- *Gu, X., Zhang, J., Guo, S., Zhang, Y., Xu, L., Jin, R., & Li, G. (٢٠٢٥). Tiara Ni clusters for electrocatalytic nitrate reduction to ammonia with ٩٧٪ Faradaic efficiency. Journal of the American Chemical Society, ١٤٧(٢٦), ٢٢٧٨٥–٢٢٧٩٥.*

١٧- *https://doi.org/١٠.١٠٢١/jacs.٥c٠٤٩٥٠*

١٨- *Subramanian, S., Yang, K., Li, M., Sassenburg, M., Abdinejad, M., Irtem, E., Middelkoop, J., & Burdyny, T. (٢٠٢٢). Geometric catalyst utilization in zero-gap CO_2 electrolyzers. ACS Energy Letters, ٨(١), ٢٢٢–٢٢٩.*

١٩- *https://doi.org/١٠.١٠٢١/acsenergylett.٢c٠٢١٩٤ (PubMed)*

٢٠- *Reuillard, B., Blanco, M., Calvillo, L., Coutard, N., Ghedjatti, A., Chenevier, P., Agnoli, S., Otyepka, M., Granozzi, G., & Artero, V. (٢٠٢٠). Noncovalent integration of a bioinspired Ni catalyst to graphene acid for reversible electrocatalytic hydrogen oxidation. ACS Applied Materials & Interfaces, ١٢(٥), ٥٨٠٥–٥٨١١.*

٢١- *https://doi.org/١٠.١٠٢١/acsami.٩b١٨٩٢٢ (PubMed)*

٢٢- *Beiler, A. M., McCarthy, B. D., Johnson, B. A., & Ott, S. (٢٠٢٠). Enhancing photovoltages at p-type semiconductors through a redox-active metal-organic framework surface coating. Nature Communications, ١١(١), ٥٨١٩.*

٢٣- *https://doi.org/١٠.١٠٣٨/s٤١٤٦٧-٠٢٠-١٩٤٨٣-٥ (PubMed)*

٢٤- *Ghedjatti, A., Coutard, N., Calvillo, L., Granozzi, G., Reuillard, B., Artero, V., Guetaz, L., Lyonnard, S., Okuno, H., & Chenevier, P. (٢٠٢١). How do H_2 oxidation molecular catalysts assemble onto carbon nanotube electrodes? A crosstalk between electrochemical and multi-physical characterization techniques. Chemical Science, ١٢, ١٥٩١٦–١٥٩٢٧. https://doi.org/١٠.١٠٣٩/D١SC٠٥١٦٨G (RSC Publishing)*

٢٥- *Phua, Y. K., Dhammika Weerathunga, D. T., Wu, D., Kim, C., Jayawickrama, S. M., Tanaka, N., & Fujigaya, T. (٢٠٢٢). Effect of carbon nanotube-based catalyst layer surface roughness on polymer electrolyte membrane fuel cell performance. Sustainable Energy & Fuels, ٦, ٤٦٣٦–٤٦٤٤. https://doi.org/١٠.١٠٣٩/D٢SE٠٠٨٥٧B (RSC Publishing)*

٢٦- *Wang, Y.-C., Huang, W., Wan, L.-Y., Yang, J., Xie, R.-J., Zheng, Y.-P., Tan, Y.-Z., Wang, Y.-S., Zaghib, K., Zheng, L.-R., Sun, S.-H., Zhou, Z.-Y., & Sun, S.-G. (٢٠٢٢). Identification of the*

active triple-phase boundary of a non-Pt catalyst layer in fuel cells. Science Advances, ٨(٤٤), eadd٨٨٧٣. *https://doi.org/١٠.١١٢٦/sciadv.add٨٨٧٣ (PubMed)*

٢٧- *Santhosh, N. M., Gupta, S., Shvalya, V., Kosiček, M., Zavasnik, J., & Cvelbar, U. (٢٠٢٥). Advancing oxygen evolution catalysis with dual-phase nickel sulfide nanostructures. Energy & Fuels, ٣٩, ١٣٧٥–١٣٨٣.* *https://doi.org/١٠.١٠٢١/acs.energyfuels.٤c٠٥١٨٢ (MPG.PuRe)*

٢٨- *Zhu, S., Liu, T., Yu, S., Yang, H., Sun, Q., & Zheng, J. Y. (٢٠٢٣). Constructing stable MoO_x–NiS_x film via electrodeposition and hydrothermal method for water splitting. Catalysts, ١٣(١١), ١٤٢٦.* *https://doi.org/١٠.٣٣٩٠/catal١٣١١١٤٢٦ (mdpi.com)*

٢٩- *Darabi, M., Nikoorazm, M., Tahmasbi, B., & Ghorbani-Choghamarani, A. (٢٠٢٣). Immobilization of Ni(II) complex on the surface of mesoporous modified-KIT-٦ as a new, reusable and highly efficient nanocatalyst for the synthesis of tetrazole and pyranopyrazole derivatives. RSC Advances, ١٣, ١٢٥٧٢–١٢٥٨٨.*

٣٠- *https://doi.org/١٠.١٠٣٩/D٢RA٠٨٢٦٩A*

٣١- *Singh, A. S., Jindani, S., Ganguly, B., & Biradar, A. V. (٢٠٢٢). Highly regioselective tandem hydroformylation of substituted styrene using Iminophosphine rhodium complex immobilized on carbon. Journal of Industrial and Engineering Chemistry, ١١٢, ٢١٨–٢٣٢.* *https://doi.org/١٠.١٠١٦/j.jiec.٢٠٢٢.٠٥.٠١٦*

٣٢- *Ariaeinezhad, F., Mohammadnezhad, G., Akintola, O., & Plass, W. (٢٠٢٦). Synthesis of a hybrid material based on a high-surface-area magnetic Fe_3O_4@TiO_2 core–shell structure and immobilized Ni–PNP aliphatic pincer complex: study of the structural, magnetic, and antibacterial properties and nonenzymatic electrochemical sensing of glucose. Materials Advances, ٧, ٩٨٦–١٠٠٥.*

٣٣- *https://doi.org/١٠.١٠٣٩/D٥MA٠٠٧٦٢C*

٣٤- *Brunner, F. M., Neville, M. L., & Kubiak, C. P. (٢٠٢٠). Investigation of Immobilization Effects on $Ni(P^2N^2)_2$ Electrocatalysts. Inorganic Chemistry, ٥٩(٢٣), ١٦٨٧٢–١٦٨٨١.* *https://doi.org/١٠.١٠٢١/acs.inorgchem.٠c٠١٦٦٩*

٣٥- *Poienar, M., Svera, P., Taranu, B.-O., Ianasi, C., Sfirloaga, P., Buse, G., Veber, P., & Vlazan, P. (٢٠٢٢). Electrochemical*

Investigation of Nickel Phosphite Electrodes ($Ni_{11}(HPO_3)_8(OH)_6$) for Electrocatalytic Urea Oxidation Reaction. Crystals, ١٢(١٢), ١٨٠٣. https://doi.org/١٠.٣٣٩٠/cryst١٢١٢١٨٠٣

٣٦- *Bernasconi, R., Khalil, M. I., Cakmakci, D. S., Bektas, Y., Nobili, L., Magagnin, L., & Lenardi, C. (٢٠٢٢). Electrocatalytic layers for hydrogen evolution reaction based on nickel phosphides: Cost-effective fabrication and XPS characterization. Journal of Materials Science, ٥٧(٢٠), ٩٣٧٠–٩٣٨٨.* https://doi.org/١٠.١٠٠٧/s١٠٨٥٣-٠٢٢-٠٧٢٥١-٣

٣٧- *Ding, X., Liu, D., Zhao, P., Chen, X., Wang, H., Oropeza, F. E., Gorni, G., Barawi, M., García-Tecedor, M., de la Peña O'Shea, V. A., Hofmann, J. P., Li, J., Kim, J., Cho, S., Wu, R., & Zhang, K. H. L. (٢٠٢٤). Dynamic restructuring of nickel sulfides for electrocatalytic hydrogen evolution reaction. Nature Communications, ١٥(١), ٥٣٣٦.* https://doi.org/١٠.١٠٣٨/s٤١٤٦٧-٠٢٤-٤٩٠١٥-٤

٣٨- *Yoo, J. S., Bollapragada, J., Kumar, D., & Tiede, D. M. (٢٠٢٥). Investigating nickel molecular electrocatalysts for sustainable chemistry: from experimental design to materials and devices. Chemical Science, ١٦, ١٠٩٣–١١٠٥.*

٣٩- https://doi.org/١٠.١٠٣٩/D٤SC٠٦٩٥٧A

٤٠- *Gu, X., Zhang, J., Guo, S., Zhang, Y., Xu, L., Jin, R., & Li, G. (٢٠٢٥). Tiara Ni clusters for electrocatalytic nitrate reduction to ammonia with ٩٧٪ Faradaic efficiency. Journal of the American Chemical Society, ١٤٧(٢٦), ٢٢٧٨٥–٢٢٧٩٥.*

٤١- https://doi.org/١٠.١٠٢١/jacs.٥c٠٤٩٥٠

٤٢- *Yao, Q., Chen, J., Xiao, S., Zhang, Y., & Zhou, X. (٢٠٢١). Selective electrocatalytic reduction of nitrate to ammonia with nickel phosphide. ACS Applied Materials & Interfaces, ١٣(٢٦), ٣٠٤٥٨–٣٠٤٦٧.* https://doi.org/١٠.١٠٢١/acsami.٠c٢٢٣٣٨

٤٣- *Wu, Z.-Y., Karamad, M., Yong, X., Huang, Q., Cullen, D. A., Zhu, P., Xia, C., Xiao, Q., Shakouri, M., Chen, F.-Y., Kim, J. Y. T., Xia, Y., Heck, K., Hu, Y., Wong, M. S., Li, Q., Gates, I., Siahrostami, S., & Wang, H. (٢٠٢١). Electrochemical ammonia synthesis via nitrate reduction on Fe single atom catalyst. Nature Communications, ١٢(١), ٢٨٧٠.* https://doi.org/١٠.١٠٣٨/s٤١٤٦٧-٠٢١-٢٣١١٥-x

٤٤- *Liao, W., Wang, J., Ni, G., Liu, K., Liu, C., Chen, S., Wang, Q., Chen, Y., Luo, T., Wang, X., Wang, Y., Li, W., Chan, T.-S., Ma, C., Li, H., Liang, Y., Liu, W., Fu, J., Xi, B., & Liu, M. (٢٠٢٤). Sustainable conversion of alkaline nitrate to ammonia at activities greater than ٢ A cm⁻². Nature Communications, ١٥(١), ١٢٦٤.*

٤٥- https://doi.org/١٠.١٠٣٨/s٤١٤٦٧-٠٢٤-٤٥٥٣٤-٢

٤٦- *Liu, K., Li, H., Xie, M., Wang, P., Jin, Z., Liu, Y., Zhou, M., Li, P., & Yu, G. (٢٠٢٤). Thermally enhanced relay electrocatalysis of nitrate-to-ammonia reduction over single-atom-alloy oxides. Journal of the American Chemical Society, ١٤٦(١١), ٧٧٧٩–٧٧٩٠. https://doi.org/١٠.١٠٢١/jacs.٤c٠٠٤٢٩*

٤٧- *Wang, W., Chen, J., & Tse, E. C. M. (٢٠٢٣). Synergy between Cu and Co in a layered double hydroxide enables close to ١٠٠٪ nitrate-to-ammonia selectivity. Journal of the American Chemical Society, ١٤٥(٤٩), ٢٦٦٧٨–٢٦٦٨٧.*

٤٨- https://doi.org/١٠.١٠٢١/jacs.٣c٠٨٠٨٤

٤٩- *Li, P., Li, R., Liu, Y., Xie, M., Jin, Z., & Yu, G. (٢٠٢٣). Pulsed nitrate-to-ammonia electroreduction facilitated by tandem catalysis of nitrite intermediates. Journal of the American Chemical Society, ١٤٥(١١), ٦٤٧١–٦٤٧٩.*

٥٠- https://doi.org/١٠.١٠٢١/jacs.٣c٠٠٣٣٤

٥١- *Zhang, R., Li, C., Cui, H., Wang, Y., Zhang, S., Li, P., Hou, Y., Guo, Y., Liang, G., Huang, Z., Peng, C., & Zhi, C. (٢٠٢٣). Electrochemical nitrate reduction in acid enables high-efficiency ammonia synthesis and high-voltage pollutes-based fuel cells. Nature Communications, ١٤(١), ٨٠٣٦. https://doi.org/١٠.١٠٣٨/s٤١٤٦٧-٠٢٣-٤٣٨٩٧-٦*